室蘭工業大学
学術資源アーカイブ
Muroran Institute of Technology Academic Resources Archive

Two-Dimensional Full-Vectorial Finite Element Analysis of NRD Guide Devices

著者	Tsuji Yasuhide, Morimoto Keita, Iguchi Akito, Kashiwa Tatsuya, Nishiwaki Shinji
journal or publication title	IEEE MICROWAVE AND WIRELESS COMPONENTS LETTERS
volume	31
number	4
page range	345-348
year	2021
URL	http://hdl.handle.net/10258/00010460

doi: info:doi/10.1109/LMWC.2021.3060179

Two-Dimensional Full-Vectorial Finite Element Analysis of NRD Guide Devices

Yasuhide Tsuji, *Senior Member, IEEE,* Keita Morimoto, *Student Member, IEEE,* Akito Iguchi, *Member, IEEE,* Tatsuya Kashiwa, *Senior Member, IEEE,* and Shinji Nishiwaki, *Non-Member, IEEE*

***Abstract*—Non-radiative dielectric waveguide (NRD guide) is a promising platform for realizing compact millimeter waveguide circuits. NRD guide devices have been simulated by several numerical simulation approaches so far and these approaches basically treat three dimensional structure because electric and magnetic fields in NRD guides vary in whole directions. In this paper, we propose a two-dimensional full-vectorial finite element analysis for efficient simulation of NRD guide devices.**

***Index Terms*—Non-radiative dielectric waveguide (NRD guide), finite element method (FEM), full-vectorial analysis.**

I. Introduction

In recent progress of wireless communication systems, such as 5G and beyond 5G, utilization of the higher frequency band is extensively explored. Non-radiative dielectric waveguide (NRD guide) is one of promising platforms, in which compact millimeter-wave circuit can be realized thanks to its non-radiative nature[1]-[12]. In order to design high performance devices with novel functions, several kinds of optimization technique for electromagnetic wave devices have been proposed and developed[13]-[16]. In such optimization techniques, numerical simulation is required to be iteratively carried out to optimize a lot of design variables, thus, improvement of the computational efficiency of the simulation is highly desired. NRD guide devices have been simulated by several numerical simulation approaches so far and these approaches basically treat three dimensional structure[16] because electric and magnetic fields of non-radiative modes in NRD guides vary in whole x-, y-, and z-directions even if the structure is uniform in the direction vertical to metal plates. These field variations are not the same for all the electromagnetic field components even along the uniform direction. Thus, the non-radiative modes in NRD guides are hybrid modes and mode coupling between different polarization modes occurs if the structure varies arbitrarily on the circuit plane. Therefore, three-dimensional analysis has been employed so far. In this paper, we first propose two-dimensional full-vectorial finite element analysis for efficient simulation of NRD guide devices with uniform structure in the vertical direction to metal plates. It is shown that our formulation can treat polarization coupling between LSM_{01} and LSE_{01} modes even in the two-dimensional analysis.

Manuscript received December 5, 2020; revised February 1, 2021. This work was supported by JSPS (Japan) KAKENHI Grant Number 18K04276. *(Corresponding author: Yasuhide Tsuji)*

Y. Tsuji, K. Morimoto, and A. Iguchi are with Muroran Institute of Technology, Japan, e-mail: y-tsuji@mmm.muroran-it.ac.jp.

T. Kashiwa is with Kitami Institute of Technology, Japan.

S. Nishiwaki is with Kyoto University, Japan.

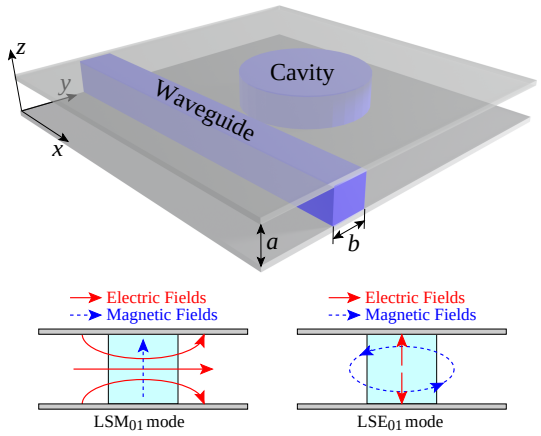

Fig. 1. Image of NRD guide circuit and non-radiative modes (LSM_{01}, LSE_{01}) of the NRD guide.

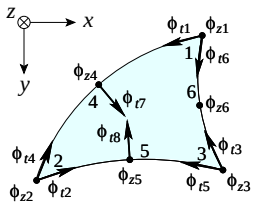

Fig. 2. Edge/Nodal hybrid element with curved boundary.

II. Two-dimensional Full-Vectorial Finite Element Method

Considering an NRD guide device as shown in Fig. 1, propagating behavior in NRD guides is governed by Maxwell's equation, and its functional for waveguide analysis by finite element method is written as follows:

$$F = \iiint \left[(\nabla \times \boldsymbol{H}^*) \cdot \left(\frac{1}{\varepsilon_r} \nabla \times \boldsymbol{H} \right) - k_0^2 \boldsymbol{H}^* \cdot \boldsymbol{H} \right] dV - \iint \left\{ \boldsymbol{H}^* \cdot \left(\boldsymbol{i}_n \times \frac{1}{\varepsilon_r} \nabla \times \boldsymbol{H} \right) \right\} dS. \quad (1)$$

where k_0 is a free-space wavenumber and ε_r is a relative permittivity distribution. In this type of NRD guide devices, because of the uniformity of the structure along the z-direction, electric and magnetic fields, E_i and H_i $(i = x, y, z)$ in LSM_{n1} and LSE_{n1} modes $(n = 0, 1, \cdots)$ can be expressed as follows:

$$E_x = \phi_x(x, y) \sin\left(\frac{\pi}{a} z\right), \quad H_x = \psi_x(x, y) \cos\left(\frac{\pi}{a} z\right),$$

$$E_y = \phi_y(x,y)\sin\left(\frac{\pi}{a}z\right), \quad H_y = \psi_y(x,y)\cos\left(\frac{\pi}{a}z\right),$$
$$E_z = \phi_z(x,y)\cos\left(\frac{\pi}{a}z\right), \quad H_z = \psi_z(x,y)\sin\left(\frac{\pi}{a}z\right).$$

In order to obtain finite element expression for waveguide analysis, discretizing computational domain into curvilinear edge/nodal hybrid elements [17]-[19] as shown in Fig. 2, approximating magnetic field component by

$$\begin{aligned}\boldsymbol{\psi}(x,y) &= \left(\boldsymbol{i}_x\{U\}^T + \boldsymbol{i}_y\{V\}^T\right)\{\psi_t\} + \boldsymbol{i}_z\{N\}^T\{\psi_z\} \\ &= \{\boldsymbol{N}\}^T\{\psi\} \end{aligned} \tag{2}$$

and applying variational principle, then, the following linear equation is derived:

$$\left([K] - k_0^2[M]\right)\{\psi\} = \{u\} \tag{3}$$

$$[K] = \begin{bmatrix} [K_{tt}] & [K_{tz}] \\ [K_{zt}] & [K_{zz}] \end{bmatrix}, \quad [M] = \begin{bmatrix} [M_{tt}] & [0] \\ [0] & [M_{zz}] \end{bmatrix},$$
$$\{\psi\} = \begin{bmatrix} \{\psi_t\} \\ \{\psi_z\} \end{bmatrix}, \quad \{u\} = \begin{bmatrix} \{u_t\} \\ \{u_z\} \end{bmatrix}$$

where $\{U\}$, $\{V\}$ are shape functions of edge element, $\{N\}$ is a shape function of nodal element, and the submatrices are defined by

$$\begin{aligned}
[K_{tt}] &= \sum_e \iint_e \left[\left(p_x\{V\}\{V\}^T + p_y\{U\}\{U\}^T\right)\left(\frac{\pi}{a}\right)^2 \right. \\
&\quad \left. + p_z\left(\frac{\partial\{V\}}{\partial x} - \frac{\partial\{U\}}{\partial y}\right)\left(\frac{\partial\{V\}^T}{\partial x} - \frac{\partial\{U\}^T}{\partial y}\right)\right] dxdy \\
[K_{tz}] &= \sum_e \iint_e \left[\left(p_x\{V\}\frac{\partial\{N\}^T}{\partial y} + p_y\{U\}\frac{\partial\{N\}^T}{\partial x}\right)\left(\frac{\pi}{a}\right)\right] dxdy \\
[K_{zt}] &= \sum_e \iint_e \left[\left(p_x\frac{\partial\{N\}}{\partial y}\{V\}^T + p_y\frac{\partial\{N\}}{\partial x}\{U\}^T\right)\left(\frac{\pi}{a}\right)\right] dxdy \\
[K_{zz}] &= \sum_e \iint_e \left[\left(p_y\frac{\partial\{N\}}{\partial x}\frac{\partial\{N\}^T}{\partial x} + p_x\frac{\partial\{N\}}{\partial y}\frac{\partial\{N\}^T}{\partial y}\right)\right] dxdy \\
[M_{tt}] &= \sum_e \iint_e \left[q_x\{U\}\{U\}^T + q_y\{V\}\{V\}^T\right] dxdy \\
[M_{zz}] &= \sum_e \iint_e q_z\{N\}\{N\}^T dxdy \\
\{u\} &= \int_\Gamma \{\{\boldsymbol{N}\}\cdot(\boldsymbol{i}_n \times [p]\nabla \times \boldsymbol{H})\}\, d\Gamma, \quad [p] = \mathrm{diag}\{p_x, p_y, p_z\}
\end{aligned}$$

where Γ is the input boundary, and if perfectly matched layer (PML)[20] is placed outside the real computational domain to express semi-infinite region[21], p_i, q_i $(i = x, y, z)$ is defined as follows:

$$p_x = \frac{1}{\varepsilon_r}\cdot\frac{s_x}{s_y}, \quad p_y = \frac{1}{\varepsilon_r}\cdot\frac{s_y}{s_x}, \quad p_z = \frac{1}{\varepsilon_r}\cdot\frac{1}{s_x s_y}$$
$$q_x = \frac{s_y}{s_x}, \quad q_y = \frac{s_x}{s_y}, \quad q_z = s_x s_y,$$

and s_i is stretching parameters along the i-direction in PML region.

Assuming the inputting direction is the x-direction, boundary condition at Γ where eigenmode with a propagation constant, β, is launched is given by

$$\{u\} = \begin{bmatrix} [B_{tx}] & [B_{ty}] & [0] \\ [B_{zx}] & [0] & [B_{zz}] \end{bmatrix} \begin{bmatrix} \{\psi_x\}_\Gamma \\ \{\psi_y\}_\Gamma \\ \{\psi_z\}_\Gamma \end{bmatrix} \tag{4}$$

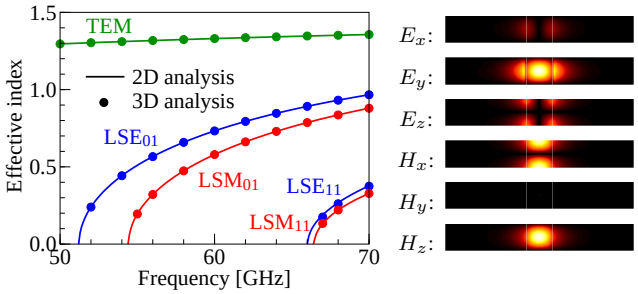

Fig. 3. Dispersion relation of guided modes in an NRD guide and field distribution of LSM_{01} mode at frequency of 60 GHz.

where

$$\boldsymbol{\psi}_\Gamma = \boldsymbol{i}_x\{N\}^T\{\psi_x\}_\Gamma + \boldsymbol{i}_y\{V\}^T\{\psi_y\}_\Gamma + \boldsymbol{i}_z\{N\}^T\{\psi_z\}_\Gamma \tag{5}$$

$$\begin{aligned}
[B_{tx}] &= \sum_\Gamma \int_\Gamma \frac{1}{\varepsilon_r}\{V\}\frac{\partial\{N\}^T}{\partial y}dy \\
[B_{ty}] &= \sum_\Gamma \int_\Gamma j\beta\frac{1}{\varepsilon_r}\{V\}\{V\}^T dy \\
[B_{zx}] &= \sum_\Gamma \int_\Gamma -\frac{1}{\varepsilon_r}\left(\frac{\pi}{a}\right)\{N\}\{N\}^T dy \\
[B_{zz}] &= \sum_\Gamma \int_\Gamma j\beta\frac{1}{\varepsilon_r}\{N\}\{N\}^T dy
\end{aligned}$$

. LSM mode in the input port is obtained by solving the following wave equation:

$$\frac{\partial}{\partial y}\left(\frac{1}{\varepsilon_r}\frac{\partial\psi_z}{\partial y}\right) + \left(k_0^2 - \frac{\beta^2 + (\pi/a)^2}{\varepsilon_r}\right)\psi_z = 0 \tag{6}$$

$$\begin{aligned}
\phi_x &= \frac{1}{j\omega\varepsilon_0\varepsilon_r}\left(\frac{\pi}{a}\right)\frac{\partial\psi_z}{\partial y} & \psi_x &= \frac{1}{j\beta}\left(\frac{\pi}{a}\right)\psi_z \\
\phi_y &= \frac{1}{\omega\varepsilon_0\varepsilon_r\beta}\left\{\beta^2 + \left(\frac{\pi}{a}\right)^2\right\}\psi_z & \psi_y &= 0 \\
\phi_z &= \frac{1}{\omega\varepsilon_0\varepsilon_r\beta}\left(\frac{\pi}{a}\right)\frac{\partial\psi_z}{\partial y}.
\end{aligned}$$

where ε_0 is the permittivity of vacuum and ω is the angular frequency.

Although wave equation for LSE mode is given by

$$\frac{\partial}{\partial y}\left(\frac{\partial\phi_z}{\partial y}\right) + \left(\varepsilon_r k_0^2 - \left(\beta^2 + (\pi/a)^2\right)\right)\phi_z = 0, \tag{7}$$

both LSE and LSM modes can be treated by (3) because (3) is derived from full-vectorial expression (1).

III. Numerical Examples

A. Guided Mode Analysis

In order to confirm the validity of two-dimensional finite element analysis, first, we calculate the guided modes in the NRD guide with height of $a = 2.25$ mm and width of $b = a$. The relative permittivity of the dielectric material is assumed to be $\varepsilon_r = 2.2$, and surrounding material is assumed to be air with relative permittivity of $\varepsilon_{\mathrm{air}} = 1$. Figure 3 shows the results obtained by two-dimensional (2D)

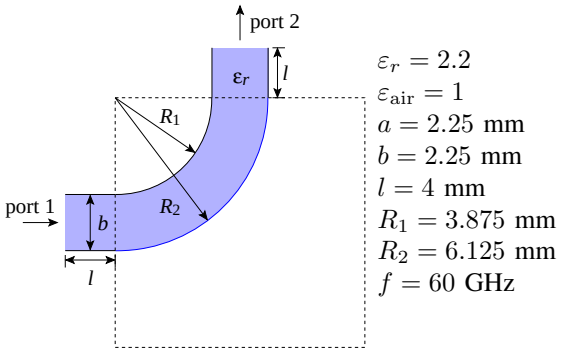

Fig. 4. Top view of simple 90 degree bend.

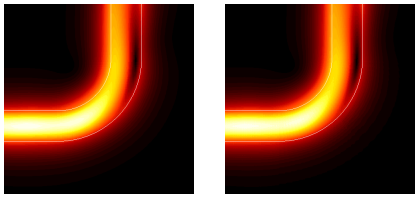

(a) (b)

Fig. 5. Propagating field ($|H_z|$) in the simple 90 degree bend calculated by (a) 2D FEM and (b) 3D FEM.

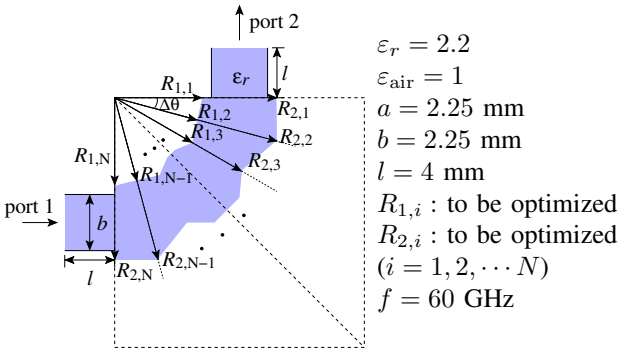

Fig. 6. Top view of design model of 90 degree bend.

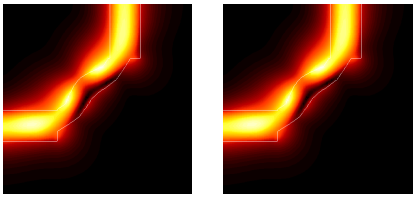

(a) (b)

Fig. 7. Propagating field ($|H_z|$) in the designed 90 degree bend calculated by (a) 2D FEM and (b) 3D FEM.

analysis and three-dimensional (3D) analysis. In this analysis, the results in 2D analysis are analytically calculated and those in 3D analysis are obtained by FEM with edge/nodal hybrid triangular elements [19]. We can see that both results are in good agreement.

B. Wave Propagation Analysis

Next, we consider a waveguide bend as shown in Fig. 4. The height and width of the input and output waveguides are $a = 2.25$ mm and $b = a$, respectively. The inner and outer radius of the waveguide bend are $R_1 = 3.875$ mm and $R_2 = 6.125$ mm, respectively. We consider the case that the LSM_{01} mode with operating frequency of 60 GHz is launched into port 1. Figure 5 shows the propagating fields obtained by 2D FEM and 3D FEM [22]. We can see that both results are in good agreement and the normalized transmission power as LSM_{01} is only 0.21 in both analyses due to mode conversion from LSM_{01} to LSE_{01}. In this analysis, only 0.4 GB of memory and 4.5 seconds of computational time are required in 2D analysis, whereas about 20 GB of memory and 109 seconds of computational time are required in 3D analysis using a PC with Intel(R) Xeon(R) CPU E5-2660 v4 @ 2.00GHz. In 2D analysis, we can get sufficient numerical convergence using even fewer discretization. In this 3D analysis, the numercal accuracty is within relative error of about 0.5% in the normalized transmission power. To obtain more accurate results, further computational cost is required.

Finally, we consider a waveguide bend as shown in Fig. 6. The shape of this bend is represented by 20 control points ($N = 10$) placed on the material boundary and these control points are optimized by the simple gradient method where the sensitivities with respect to the design variables are calculated by forward difference formula. In this example, the control points are placed at equal intervals in the angular direction and only the distance from the center is designed. Figure 7 shows the propagating fields in the designed waveguide bend obtained by 2D FEM and 3D FEM. We can see that both results are in good agreement and the normalized transmission power as LSM_{01} is improved up to 0.97 because mode conversion to LSE_{01} mode can be suppressed. In Table I, S-parameters are listed for two bends shown in Fig. 4 and Fig. 6.

TABLE I
COMPARISON OF S-PARAMETERS AT $f = 60$ GHZ OBTAINED BY 2D-FEM AND 3D-FEM FOR BEND SHOWN IN FIG. 4 AND OPTIMIZED BEND SHOWN IN FIG. 6.

S-parameter	Output mode	Bend in Fig. 4		Bend in Fig. 6	
		2D	3D	2D	3D
$\lvert S_{21}\rvert$ [dB]	LSM_{01}	-6.74	-6.59	-0.13	-0.15
	LSE_{01}	-1.04	-1.05	-16.1	-17.1
$\lvert S_{11}\rvert$ [dB]	LSM_{01}	-35.3	-32.2	-25.1	-21.1
	LSE_{01}	-34.1	-34.2	-23.0	-21.5

IV. CONCLUSION

We proposed two-dimensional finite element analysis of NRD guide devices with uniformity along the vertical direction and derived the formulation by using edge/nodal hybrid triangular elements. To show the validity and usefulness of this approach, two kinds of waveguide bends were calculated by the proposed 2D FEM and the conventional 3D FEM and the good agreement between both results was confirmed. We think this 2D FEM is very useful in future toplogy optimal design of NRD guide devices.

REFERENCES

[1] T. Yoneyama and S. Nishida, "Nonradiative dielectric waveguide for millimeter-wave integrated circuits," *IEEE Trans. Microw. Theory Tech.*, vol.MTT-29, no. 11, pp. 1188–1192, Dec. 1981.

[2] T. Yoneyama and S. Nishida, "Nonradiative dielectric waveguide T-juctions for millimeter-wave application," *IEEE Trans. Microw. Theory Tech.*, vol.MTT-33, no. 11, pp. 1239–1241, Nov. 1985.
[3] T. Yoneyama, S. Nishida, and I. Tamaki, "Analysis and measurements of nonradiative dielectric waveguide bends," *IEEE Trans. Microw. Theory Tech.*, vol.MTT-34, no. 8, pp. 876–882, Aug. 1986
[4] T. Yoneyama, "Millimeter-wave integrated circuits using nonradiative dielectric waveguide," *IEICE Trans. Electron.(Jananese Edition)*, vol.J73-C-I, no.3, pp. 87–94, Mar. 1990.
[5] K. Wu and L. Han, "Hybrid integration technology of planar circuits and NRD-guide for cost-effective microwave and millimeter-wave applications," *IEEE Trans. Microw. Theory Tech.*, vol. 45, no. 6, pp. 946–954, June 1997.
[6] F. Boone and K. Wu, "Mode conversion and design consideration of integrated nonradiative dielectric (NRD) components and discontinuities," *IEEE Trans. Microw. Theory Tech.*, vol. 48, no. 4, pp. 482–492, Apr. 2000.
[7] F. Kuroki, K. Wada, and T. Yoneyama, "Low-Loss and small-sized NRD guide ring resonators and their application to channel dropping filter at 60 GHz," *IEICE Trans. Electron.*, vol. E86-C, no. 8, pp. 1601–1606, Aug. 2003.
[8] J. Y. Lee, J. H. Lee, C. H. Im, H. S. Kim, K. Choi, and H.-K. Jung, "Selection of proper modes of an NRD guide using a perturbing boundary," *IEEE Trans. Magnet.*, vol. 39, no. 3, pp. 1246–1249, May 2003.
[9] D. Li, Y. Cassivi, P. Yang, and K. Wu, "Analysis and design of bridged NRD-guide coupler for millimeter-wave applications," *IEEE Trans. Microw. Theory Tech.*, vol. 53, no. 8, pp. 2546–2551, Aug. 2005.
[10] F. Kuroki, K. Makoto, and T. Yoneyama, "A Transition between NRD guide and microstrip line at 60 GHz," *IEICE Trans. Electron.*, vol. E88-C, no. 10, pp. 1968–1972, Oct. 2005.
[11] Y. Kamo, K. Munetou, and F. Kuroki, "Transmission loss evaluation of 94GHz NRD guide toward THz-band dielectric integrated circuits," *2016 IEEE International Symposium on Radio-Frequency Integration Technology (RFIT)*, Aug. 2016.
[12] E. Polat, R. Reese, M. Jost, C. Schuster, M. Nickel, R. Jakoby, and H. Maune, "Tunable liquid crystal filter in nonradiative dielectric waveguide technology at 60 GHz," *IEEE Microw. Wireless Compon. Lett.*, vol. 29, no. 1, Jan. 2019.
[13] J. S. Jensen and O. Sigmund, "Systematic design of photonic crystal structures using topology optimization: Low-loss waveguide bends," *Appl. Phys. Lett.*, vol. 84, pp. 2022–2024, Mar. 2003.
[14] Y. Tsuji, K. Hirayama, T. Nomura, K. Sato, and S. Nishiwaki, "Design of optical circuit devices based on topology optimization," *IEEE Photon. Technol. Lett.*, vol. 18, no. 7, pp. 850–852, Apr. 2006.
[15] Y. Tsuji, and K. Hirayama, "Design of optical circuit devices using topology optimization method with function-expansion-based refractive index distribution," *IEEE Photon. Technol. Lett.*, vol. 20, no. 12, pp. 982–984, June 2008.
[16] N. Uchida, S. Nishiwaki, K. Izui, M. Yoshimura, and T. Nomura, "Topology Optimization of Electromagnetic Waveguides," *8-th World Congress on Structural and Multidisciplinary Optimization*, June 2009.
[17] J. C. Nedelec, "Mixed finite elements in R3," *Numer. Math.*, vol. 35, pp. 315–341, Sep. 1980.
[18] J.-F. Lee, D.-K. Sun, and Z. J. Cendes, "Full-wave analysis of dielectric waveguides using tangential vector finite elements," *IEEE Trans. Microw. Theory Tech.*, vol. 39, no. 8, pp. 1262–1271, Aug. 1991.
[19] M. Koshiba and Y. Tsuji, "Curvilinear hybrid edge/nodal elements with triangular shape for guidedwave problems," *J. Lightw. Technol.*, vol. 18, no. 5, pp. 737–743, May 2000.
[20] F. L. Texeira and W. C. Chew, "General closed-form PML constitutive linear media," *IEEE Microwave Guided Wave Lett., vol. 8, pp. 223–225*, June 1998.
[21] Y. Tsuji and M. Koshiba, "Finite element method using port truncation by perfectly matched layer boundary conditions for optical waveguide discontinuity problems," *J. Lightw. Technol.*, vol. 20, no. 3, pp. 463–468, Mar. 2002.
[22] T. Yasui, Y. Tsuji, J. Sugisaka, and K. Hirayama, "Design of three-dimensional optical circuit devices by using topology optimization method with function-expansion-based refractive index distribution," *J. Lightw. Technol.*, vol. 31, no. 23, pp. 3765–3770, Dec. 2013.